Journal of Applied Electrochemistry **32**: 339–347, 2002.

Polarization effects in electrolyte/electrode-supported solid oxide fuel cells

S.H. CHAN and Z.T. XIA
Fuel Cell Strategy Research Programme, School of Mechanical and Production Engineering, Nanyang Technological University, Singapore 639798

Received 8 August 2001; accepted in revised form 13 November 2001

Key words: electrode-supported fuel cell, Knudsen diffusion, polarization, solid oxide fuel cell

Abstract

The effects of activation, ohmic and concentration polarization on the overall polarization in solid oxide fuel cells are presented. A complete analysis was conducted based on thermodynamic principles for the calculation of cell voltage. Treating the fuel cell as a control volume, the irreversibility term in a steady flow thermodynamic system was related to the overall polarization. The entropy production was calculated and related to the lost work of the fuel cell, while the heat loss from the cell was determined from the entropy balance. To generalize the cell voltage–current density expression, the Butler–Volmer model was used in the calculation of activation polarization and both ordinary and Knudsen diffusions were considered in the calculation of concentration polarization. The overall cell resistance was deduced from the generalized cell voltage–current density expression. The concentration resistance at the anode can be minimized by humidifying the hydrogen with an appropriate amount of water, depending on the thickness of the anode used. Comparison of polarization effects on the cell performance between the electrolyte-supported and anode-supported cells showed that the latter would give a better cell performance.

List of symbols

C	concentration (mol m^{-3})
D	diffusion coefficient (m^2 s^{-1})
E	voltage (V)
E_o	open circuit voltage (V)
F	faradaic constant (96 485 C mol^{-1})
$\overline{g}$	molar Gibbs free energy (J mol^{-1})
G	Gibbs free energy (J)
$\overline{h}$	molar enthalpy (J mol^{-1})
i	current density (A m^{-2})
i_n	transfer current density per unit of active area (A m^{-2})
i_o	apparent exchange current density (A m^{-2})
i_{oo}	true internal exchange current density (A m^{-2})
J	flux (mol s^{-1})
K	equilibrium constant
l	thickness (m)
l_e	electrolyte thickness (m)
n	number of moles
p	partial pressure (Pa)
Q	heat (J)
$\dot{Q}$	heat transfer rate (J s^{-1})
$\overline{r}$	average pore radius (m)
$\overline{R}$	universal gas constant (8.314 J mol^{-1} K^{-1})
R	area-specific resistance (Ω m^{-2})
R_e	electrolyte area-specific ohmic resistance (Ω m^{-2})
R_{conc}	area-specific concentration resistance (Ω m^{-2})
$\overline{s}$	molar entropy (J mol^{-1} K^{-1})
S_t	active area per unit volume (m^2 m^{-3})
$\dot{W}$	electrical power (J s^{-1})
W_{el}	electrical work (J)
W_{lost}	lost work (J)
T	temperature (K)
z	the number of electrons transferred per oxide ion

Greek letters

β	transfer coefficient
ε	porosity
η	polarization (V)
η_{act}	activation polarization (V)
η_{conc}	concentration polarization (V)
η_{ohm}	ohmic polarization (V)
ρ	resistivity (Ω m)
σ	entropy production (J mol^{-1} K^{-1})
$\dot{\sigma}$	rate of entropy production (J mol^{-1} K^{-1} s^{-1})
ξ	tortuosity

Subscripts

a	anode
c	cathode
cv	control volume
el	electronic
H_2	hydrogen
H_2O	water vapour
i	mixture component

io ionic
k Knudsen diffusion
N_2 nitrogen
O_2 oxygen
p products
r reactants
(eff) effective
(eq) equilibrium

Superscripts
o standard condition
I inlet condition

1. Introduction

The demand for high-efficiency/low-emissions power generation systems is becoming increasingly important. Optimization of the system efficiency and process operation is therefore a major task in system development. Traditionally, power plants are based on vapour power cycles or gas power cycles for power generation; the maximum thermal efficiencies of such plants are limited by the Carnot principle. However, due to the synergetic effect of solid oxide fuel cell (SOFC) and gas turbine (GT) technologies, an integrated SOFC-GT power system has been identified as an advanced technology for future power generation. Many studies have shown that, when this integrated system is based on a more complex gas turbine cycle, electrical efficiencies of 70% (net AC/LHV) or higher can be expected [1, 2]. These studies are based on the first law of thermodynamics in conjunction with the techno-economical assessment. On the other hand, there are increasingly more researchers applying the second law of thermodynamics to the analysis of overall plant efficiency associated with the calculation of the exergy at each node of the thermodynamic system. This allows exergy destruction in each system component to be determined so that the improvement of particular system component or process with high exergy destruction/losses can be focused on [3, 4]. Hence, there is a need to use a more complete polarization model of SOFC to characterize the SOFC stack, which contributes to about three quarters of the total electrical power output in an optimized integrated SOFC-GT power plant. With a more reliable polarization model, the heat generation and entropy production of the SOFC stack can be estimated; this provides useful information for heat management and system optimization of the plant.

The objectives of this study are: (i) development of a generalized cell voltage–current density expression which relates the thermodynamic irreversibility to the polarization, (ii) minimisation of the anode concentration resistance, and (iii) comparative study of the performance between the electrolyte-supported fuel cell and the anode-supported fuel cell.

2. Thermodynamic principles

Treating the fuel cell as a control volume and combining the steady flow energy equation and entropy balance equation give

$$W_{\mathrm{cv}} = -\left[\sum_{\mathrm{i}} (n_{\mathrm{i}}\overline{g}_{\mathrm{i}})_{\mathrm{P}} - \sum_{\mathrm{i}} (n_{\mathrm{i}}\overline{g}_{\mathrm{i}})_{R}\right] - T\sigma_{\mathrm{cv}} \tag{1}$$

where $\overline{g}_{\mathrm{i}}(T, p_{\mathrm{i}}) = \overline{h}_{\mathrm{i}}(T) - T\overline{s}_{\mathrm{i}}(T, p_{\mathrm{i}})$ or $\overline{g}_{\mathrm{i}}(T, p_{\mathrm{i}}) = \overline{g}_{\mathrm{i}}(T) + \overline{R}T \ln p_{\mathrm{i}}^{\mathrm{I}}/p_{\mathrm{o}}$

Since there is no mechanical work involved in the fuel cell, W_{cv} is naturally the electrical work done by the fuel cell. That is,

$$W_{\mathrm{el}} = zFE = -\left[\sum_{\mathrm{i}} (n_i\overline{g}_{\mathrm{i}})_{\mathrm{P}} - \sum_{\mathrm{i}} (n_{\mathrm{i}}\overline{g}_{\mathrm{i}})_{R}\right] - T\sigma_{\mathrm{cv}} \tag{2}$$

$$zFE = -\Delta G^{\circ} - \left[\sum_{i}\left(n_{\mathrm{i}}\overline{R}T \ln\frac{p_{\mathrm{i}}^{\mathrm{I}}}{p_{\mathrm{o}}}\right)_{\mathrm{P}} - \sum_{i}\left(n_{\mathrm{i}}\overline{R}T \ln\frac{p_{\mathrm{i}}^{\mathrm{I}}}{p_{\mathrm{o}}}\right)_{R}\right] - T\sigma_{\mathrm{cv}} \tag{3}$$

where $-\Delta G^{\circ} = \overline{R}T \ln K(T)$

For a H_2–O_2 fuel cell with known partial pressures of reactants and products, the cell voltage takes the form:

$$E = \frac{\overline{R}T}{2F} \ln K - \frac{\overline{R}T}{4F} \ln\left[\left(\frac{{p_{\mathrm{H_2O}}^{\mathrm{I}}}^2 \times p_{\mathrm{o}}}{{p_{\mathrm{H_2}}^{\mathrm{I}}}^2 \times p_{\mathrm{O_2}}^{\mathrm{I}}}\right)\right] - \frac{\sigma_{\mathrm{cv}}T}{2F} \tag{4}$$

where $(\sigma_{\mathrm{cv}}T/2F) = \eta_{\mathrm{act}} + \eta_{\mathrm{ohm}} + \eta_{\mathrm{conc}}$.

The voltage drop due to entropy production is reflected by the third term of Equation 4 and is expressed as the summation of the three polarizations.

3. Electrode polarization analysis

For electrodes made of pure electronic conductors such as Pt or LSM, the reactions occur only at the electrode–electrolyte interface and the activation polarization is described by the Butler–Volmer equation:

$$\eta_{\mathrm{act}} = \frac{2\overline{R}T}{zF} \sinh^{-1}\left(\frac{i}{2i_{\mathrm{o}}}\right) \tag{5}$$

where i_{o} is the *apparent* exchange current density. However, when mixed electronic and ionic conductors (Ni/YSZ or LSM/YSZ) are used to extend the reaction sites, there will be distributions of current and overpotential within the electrodes. Thus, the charge transfer between the electronic and ionic conductors and the transport of current are modelled based on the Ohm's law and the charge balance equation. With reference to the anode structure shown in Figure 1, the following equations can be written [5, 6]:
Ohm's law for the electronic and ionic conductors:

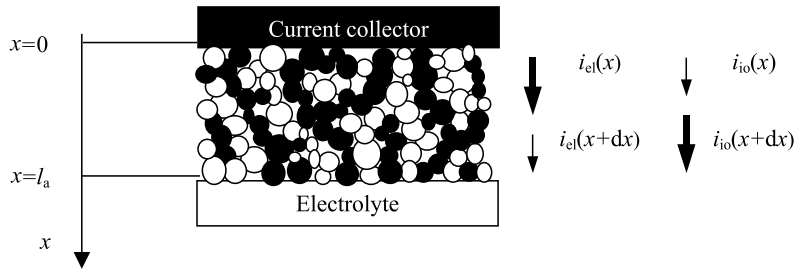

Fig. 1. Scheme of solid oxide fuel cell cermet electrode. Key: (●) electronic conductor; (○) ionic conductor.

$$\frac{dE_{el}}{dx} = \rho_{el(eff)} i_{el} \tag{6a}$$

$$\frac{dE_{io}}{dx} = \rho_{io(eff)} i_{io} \tag{6b}$$

Current balance in the electronic and ionic conductors:

$$\frac{di_{el}}{dx} = -S_t i_n \tag{7a}$$

$$\frac{di_{io}}{dx} = -\frac{di_{el}}{dx} \tag{7b}$$

The charge transfer can be described by the generalized Butler–Volmer equation as

$$i_n = i_{oo}\left\{\frac{C_r}{C_{r(eq)}}\exp\left(\beta\frac{n_e F\eta_o}{\overline{R}T}\right) - \frac{C_p}{C_{p(eq)}} \times \exp\left[-(1-\beta)\frac{n_e F\eta_o}{\overline{R}T}\right]\right\} \tag{8}$$

η_o is a function of electrode depth, x, which can be obtained by solving a set of differential equations with a very complicated solution. i_{oo} is the 'true internal' exchange current density that reflects the true reaction kinetics, which can be used in the analysis of electrode kinetics at microlevel. In contrast, i_o is obtained from curve fitting of experiment data, which lumps the effect of electrode microstructure to the reaction kinetics.

The rate of mass transport to the reaction sites in a porous electrode can be described by both the Knudsen and ordinary diffusions of gases in the pores. The former was predicted from the kinetic theory while the latter by the Chapman–Enskog theory. On the anode side, the chemical reaction occurs at the end of the diffusion path [7]. Thus,

$$J_{H_2} = -D_{a(eff)}\nabla C_{H_2} \tag{9a}$$

$$J_{H_2O} = -D_{a(eff)}\nabla C_{H_2O} \tag{9b}$$

where

$$D_{a(eff)} = \left(\frac{C_{H_2O}}{C_a}\right)D_{H_2(eff)} + \left(\frac{C_{H_2}}{C_a}\right)D_{H_2O(eff)},$$

or

$$D_{a(eff)} = \left(\frac{p_{H_2O}}{p_a}\right)D_{H_2(eff)} + \left(\frac{p_{H_2}}{p_a}\right)D_{H_2O(eff)}$$

Also,

$$D_{H_2(eff)} = \left(\frac{1}{D_{H_2,k(eff)}} + \frac{1}{D_{H_2-H_2O(eff)}}\right)^{-1}$$

and

$$D_{H_2O(eff)} = \left(\frac{1}{D_{H_2O,k(eff)}} + \frac{1}{D_{H_2-H_2O(eff)}}\right)^{-1}$$

Considering one dimensional diffusion and because $J_{H_2} = -\frac{i_{el,a}}{2F}$ and $dC_{H_2} = \frac{dp_{H_2}}{\overline{R}T}$. Thus,

$$dp_{H_2} = -\frac{\overline{R}Ti_{el,a}}{2FD_{a(eff)}}dx \tag{10}$$

When H_2 partial pressure does not change significantly, the difference between $D_{H_2(eff)}$ and $D_{H_2O(eff)}$ will be small and hence $D_{a(eff)}$ may be considered as a constant. Therefore, if the anode is a pure electronic conductor, the partial pressures of H_2 and H_2O, at the electrolyte–electrode interface can be expressed as functions of current density, i:

$$p_{H_2} = p^I_{H_2} - \frac{\overline{R}Tl_a}{2FD_{a(eff)}}i \tag{11a}$$

$$p_{H_2O} = p^I_{H_2O} + \frac{\overline{R}Tl_a}{2FD_{a(eff)}}i \tag{11b}$$

Assuming that gases diffuse through the porous anode and reactions take place only at the anode–electrolyte interface, the concentration polarization can be expressed as

$$\eta_{conc,a} = -\frac{\overline{R}T}{2F}\ln\left[\left(1-\frac{\overline{R}T}{2F}\frac{l_a}{D_{a(eff)}p^I_{H_2}}i\right)\Big/\left(1+\frac{\overline{R}T}{2F}\frac{l_a}{D_{a(eff)}p^I_{H_2O}}i\right)\right] \tag{12}$$

For a cermet electrode, reactions take place throughout the whole electrode. Therefore, the influence of concentration polarization can be very complicated, and the locations where reactions occur are determined by the combined effects of charge transfer resistance, effective electronic resistance, effective ionic resistance and effective gas resistance. However, the reactions normally occur at the sites where the total resistance reaches the minimum.

On the cathode side, the nitrogen flux is zero at the cathode side. Thus,

$$J_{O_2} = -D_c \nabla C_{O_2} + X_{O_2} \delta_{O_2} J_{O_2}, \tag{13}$$

where $\delta_{O_2} = \frac{D_{O_2,k(eff)}}{D_{O_2,k(eff)} + D_{O_2-N_2(eff)}}$.

For one dimensional diffusion:

$$J_{O_2} = -D_{O_2(eff)} \frac{dC_{O_2}}{dl} + X_{O_2} \delta_{O_2} J_{O_2} \tag{14}$$

Because $J_{O_2} = -i_{el,c}/4F$ and $dC_{O_2} = dp_{O_2}/\overline{R}T$. Therefore,

$$\frac{dp_{O_2}}{p_c - \delta_{O_2} p_{O_2}} = \frac{\overline{R}T i_{el,c}}{4F D_{O_2(eff)} p_c} dx \tag{15}$$

Hence, the partial pressure of O_2 at the cathode–electrolyte interface becomes

$$p_{O_2} = \frac{p_c}{\delta_{O_2}} - \left(\frac{p_c}{\delta_{O_2}} - p^I_{O_2}\right) \exp\left(\frac{\delta_{O_2} \overline{R}T i l_c}{4F D_{c(eff)} p_c}\right) \tag{16}$$

where $D_{c(eff)} = D_{O_2(eff)} = \frac{\varepsilon_c}{\zeta_c}\left(\frac{1}{D_{O_2,k}} + \frac{1}{D_{O_2-N_2}}\right)^{-1}$.

Assuming that reactions take place at the cathode–electrolyte interface, the concentration polarization can be expressed as

$$\eta_{conc,c} = -\frac{\overline{R}T}{4F} \ln\left[\left(\frac{p_c}{\delta_{O_2}} - \left(\frac{p_c}{\delta_{O_2}} - p^I_{O_2}\right) \times \exp\left(\frac{\overline{R}T}{4F} \frac{\delta_{O_2} l_c}{D_{c(eff)} p_c} i\right)\right) \Big/ p^I_{O_2}\right] \tag{17}$$

4. Calculation of polarization curve

To determine the voltage versus current density curve covering the whole range of cell operation, the following general expression can be used:

$$E(i) = E_o - \eta \tag{18}$$

where

$$E_o = \frac{\overline{R}T}{2F} \ln K - \frac{\overline{R}T}{4F} \ln\left(\frac{{p^I_{H_2O}}^2 \times p_o}{{p^I_{H_2}}^2 \times p^I_{O_2}}\right) \tag{18a}$$

$$\eta = \eta_{ohm} + \eta_{act,a} + \eta_{act,c} + \eta_{conc,a} + \eta_{conc,c} \tag{18b}$$

$$\eta_{ohm} = i\left(R_e + R_{ohm,a} + R_{ohm,c}\right) \tag{18c}$$

$$\eta_{act,a} = \frac{\overline{R}T}{F} \sin\ h^{-1}\left(\frac{i}{2i_{o,a}}\right) \tag{18d}$$

$$\eta_{act,c} = \frac{\overline{R}T}{F} \sin\ h^{-1}\left(\frac{i}{2i_{o,c}}\right) \tag{18e}$$

$$\eta_{conc,a} = -\frac{\overline{R}T}{2F} \ln\left[\left(1 - \frac{\overline{R}T}{2F} \frac{l_a}{D_{a(eff)} p^I_{H_2}} i\right) \Big/ \left(1 + \frac{\overline{R}T}{2F} \frac{l_a}{D_{a(eff)} p^I_{H_2O}} i\right)\right] \tag{18f}$$

$$\eta_{conc,c} = -\frac{\overline{R}T}{4F} \ln\left[\left(\frac{p_c}{\delta_{O_2}} - \left(\frac{p_c}{\delta_{O_2}} - p^I_{O_2}\right) \times \exp\left(\frac{\overline{R}T}{4F} \frac{\delta_{O_2} l_c}{D_{c(eff)} p_c} i\right)\right) \Big/ p^I_{O_2}\right] \tag{18g}$$

The entropy production per mole of H_2 consumed becomes

$$\sigma_{cv} = \frac{2F}{T} \eta \tag{19}$$

The lost work, due to the irreversible electrochemical process, can be calculated from the overall polarization:

$$W_{lost} = 2F\eta \tag{20}$$

Based on the entropy balance, the heat loss per mole of H_2 consumed from the fuel cell can be written as

$$Q_{cv} = -W_{lost} + T\left[\left(\overline{s}^o_{H_2O} - \overline{s}^o_{H_2} - \frac{1}{2}\overline{s}^o_{O_2}\right) + \frac{\overline{R}}{2} \ln\left(\frac{{p^I_{H_2}}^2 \times p^I_{O_2}}{{p^I_{H_2O}}^2 \times p_o}\right)\right] \tag{21}$$

where $\overline{s}^o_i(T) = \overline{c}_{p,i} \ln T$, which is solely a function of temperature.

Table 1 shows some experimental data extracted from the literature [8–12] focusing on the development of intermediate temperature SOFCs that operate at around 800 °C. Based on these data, the respective polarization curves can be generated. Figure 2 shows the calculated anode and cathode activation polarization. The cathode polarization is obviously higher than that of the anode due to its lower exchange current density. The activation polarization increases steeply at low current density but gradually at higher current density. Figure 3 shows the calculated concentration polarization of an anode-supported SOFC. The anode concentration polarization is much higher than that of the cathode because of the thick anode used as the cell support.

Table 1. Calculation based parameters for solid oxide fuel cell

Parameter	Value
Fuel cell operating temperature (T) / pressure (p)	1073 K/1 atm
Hydrogen humidified temperature (T_h)	298 K
Electrolyte conductivity (σ_e)	10 S m^{-1}
Transfer coefficient (β)	0.5
Number of electrons transferred per oxide ion (z)	2
Anode/cathode exchange current density ($i_{o,a}$/ $i_{o,c}$)	5300/2000 A m^{-2}
Cathode thickness (l_c)	50×10^{-6} m
Porosity (ε) / tortuosity (ξ)	30%/6
Average pore radius ($\bar{r}$)	0.5×10^{-6} m
For electrolyte-supported cell	
Electrolyte thickness (l_e)	500×10^{-6} m
Anode thickness (l_a)	50×10^{-6} m
For anode-supported cell	
Electrolyte thickness (l_e)	40×10^{-6} m
Anode thickness (l_a)	750×10^{-6} m

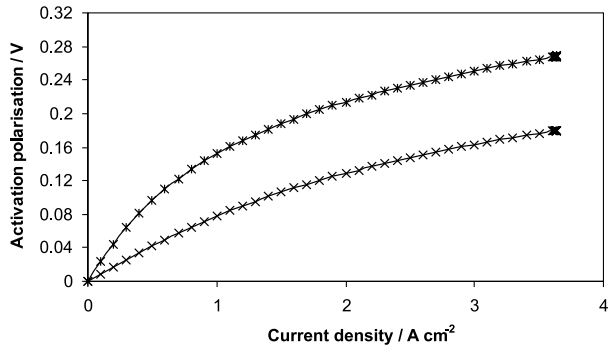

Fig. 2. Calculated activation polarization of solid oxide fuel cell. Key: (×) anode, (*) cathode.

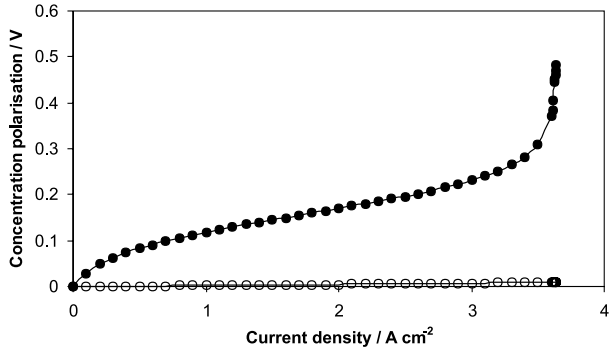

Fig. 3. Calculated concentration polarization of anode-supported solid oxide fuel cell. Key: (●) anode, (○) cathode.

5. Cell voltage and power density

Figure 4 shows the cell voltage, polarization and power density against current density of the electrolyte-supported fuel cell. The power density reaches a peak at a current density of 0.7 A cm^{-2}. The voltage and power density corresponding to this point are 0.55 V and 0.386 W cm^{-2}, respectively. The limiting current density is 1.5 A cm^{-2}. Normally, fuel cells are designed to operate slightly to the left of this point for a good compromise between cell efficiency and low capital cost, as well as the consideration of operational stability. For this case, the loss is mainly due to electrolyte ohmic polarization, though cathode and anode activation losses are also significant. It is obvious that focusing on the development of electrode-supported cells would allow the achievement of better performance than that of electrolyte-supported cells as the ohmic losses is the major determining factor in cell performance.

Figure 5 shows the cell voltage and power density versus current density of the anode-supported fuel cell. The power density reaches a peak at a current density of 2.5 A cm^{-2} and the corresponding voltage and power density are 0.415 V and 1.4 W cm^{-2}, respectively. The limiting current density is 3.6 A cm^{-2}, which is much higher than that of the electrolyte-supported cell. Therefore, the electrode material-related factors such as the catalytic activity, reaction sites, etc., which determine the magnitude of the exchange current density, are targets for improvement.

Figure 6 and 7 shows the calculated work loss and heat loss per mole of H_2 consumed, respectively. At current density of 1 A cm^{-2}, lost work (W_{lost}) and heat loss (Q_{cv}) are, respectively, 145.4 kJ (mol H_2)$^{-1}$ and 218.1 kJ (mol H_2)$^{-1}$ for the electrolyte-supported cell, and 75.3 kJ (mol H_2)$^{-1}$ and 148.1 kJ (mol H_2)$^{-1}$ for the anode-supported cell. Compared with the electrolyte-supported fuel cell operated at 1 A cm^{-2}, W_{lost} and Q_{cv} of the anode-supported fuel cell have been reduced by 48.3% and 32.1%, respectively.

Comparing the structure of the anode-supported and electrolyte-supported cells, the only difference is the thickness between the anode and the electrolyte. Therefore, keeping the same materials, it can be concluded that the performance of the anode-supported cell should be better than that of the electrolyte-supported cell.

In the derivation of the equations, we assume that the reactions occur only at electrode–electrolyte interface. These equations are obviously applicable to electrodes that are pure electronic conductors where reactions occur only at the electrode–electrolyte interface; however, their validity is questionable when they are applied to cermet electrodes. To understand the applicability of these equations in the cermet electrodes, we investigate the electrode in a microscopic level, since local polarization is different at different reaction layers.

The anode local polarization $\eta_{o,a}$ is defined as

$$\eta_{o,a} = (E_{el(eq),a} - E_{io(eq),a}) - (E_{el,a} - E_{io,a}) \tag{22}$$

where $\eta_{o,a}$ is the polarization at a particular reaction layer.

The first and second derivatives of $\eta_{o,a}$ are as follows:

$$\frac{d\eta_{o,a}}{dx} = -\left(\frac{dE_{el,a}}{dx} - \frac{dE_{io,a}}{dx}\right) = \rho_{io(eff),a} i_{io,a} - \rho_{el(eff),a} i_{el,a} \tag{23}$$

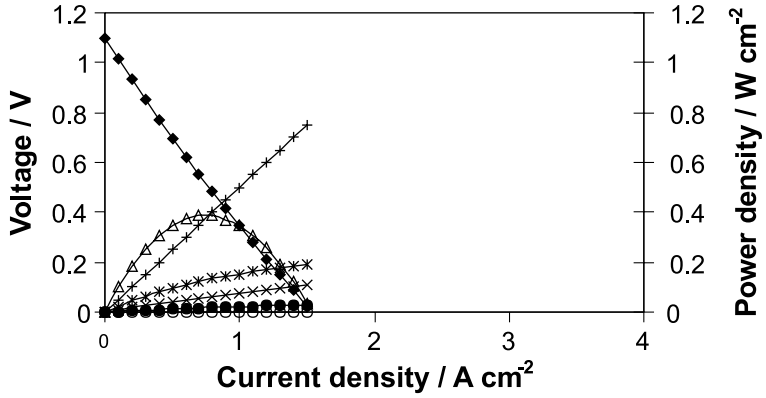

Fig. 4. Calculated cell voltage, polarization and power density against current density trace of electrolyte-supported cells. Key: cell voltage (◆), ohmic polarization (+), anode activation polarization (×), cathode activation polarization (*), anode concentration polarization (●), cathode concentration polarization (○), power density (△).

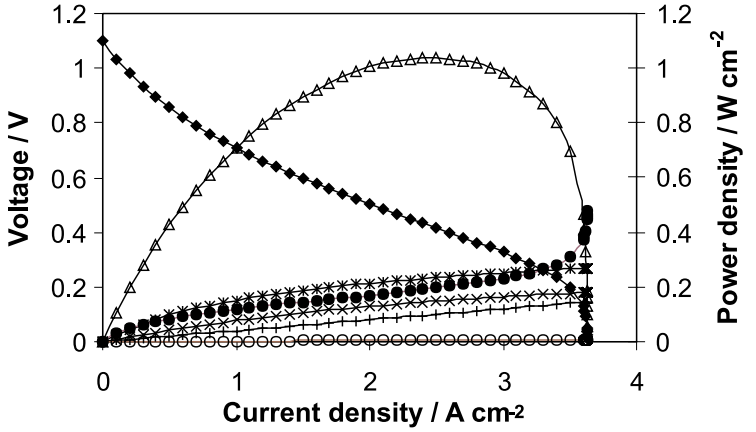

Fig. 5. Calculated cell voltage, polarization and power density against current density trace of anode-supported cells. Key: cell voltage (◆), ohmic polarization (+), anode activation polarization (×), cathode activation polarization (*), anode concentration polarization (●), cathode concentration polarization (○), power density (△).

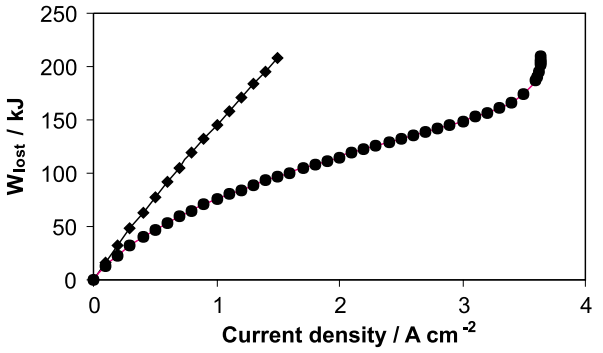

Fig. 6. Calculated lost work. Key: Electrolyte-supported cell (◆), anode-supported cell (●).

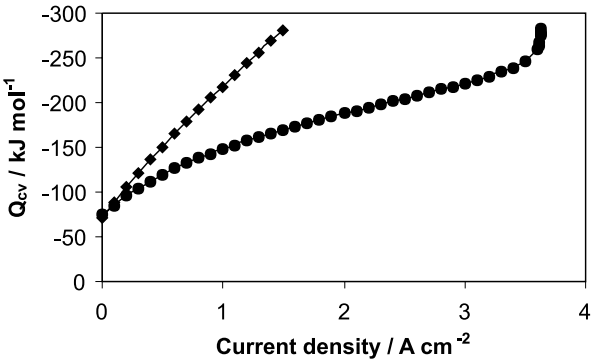

Fig. 7. Calculated heat transfer loss per mole of H_2 consumed. Key: electrolyte-supported cell (◆), anode-supported cell (●).

$$\frac{d^2\eta_{o,a}}{dx^2} = \rho_{io(eff),a}\frac{di_{io,a}}{dx} - \rho_{el(eff),a}$$
$$\frac{di_{el,a}}{dx} = \left(\rho_{el(eff),a} + \rho_{io(eff),a}\right)S_{t,a}i_{n,a}, \qquad (24)$$

where

$$i_{o,a} = i_{oo,a}\left\{\frac{C_r}{C_{r(eq)}}\exp\left(\beta\frac{n_{e,a}F\eta_{o,a}}{\overline{R}T}\right) - \frac{C_p}{C_{p(eq)}}\exp\left[-(1-\beta)\frac{n_{e,a}F\eta_{o,a}}{\overline{R}T}\right]\right\} \qquad (25)$$

For a complete analysis of the polarization, the gas transport in the anode is also considered. The concentration of the reactant and product are related to their respective partial pressure as:

$$\frac{C_r}{C_{r(eq)}} = \frac{p_{H_2}}{p^I_{H_2}} \tag{26a}$$

$$\frac{C_p}{C_{p(eq)}} = \frac{p_{H_2O}}{p^I_{H_2O}} = \frac{p_a - p_{H_2}}{p_a - p_{H_2}} \tag{26b}$$

Combining Equations 7, 10, 24 and 25, the system equations which consider all kinds of polarization can be rewritten as

$$\frac{d^2\eta_{o,a}}{dx^2} = \left(\rho_{el(eff),a} + \rho_{io(eff),a}\right) S_{t,a} i_{oo,a} \times \left\{ \frac{p_{H_2}}{p^I_{H_2}} \exp\left(\beta \frac{n_{e,a} F \eta_{o,a}}{\overline{R}T}\right) - \frac{p_a - p_{H_2}}{p_a - p^I_{H_2}} \times \exp\left[-(1-\beta)\frac{n_{e,a} F \eta_{o,a}}{\overline{R}T}\right] \right\} \tag{27a}$$

$$\frac{dp_{H_2}}{dx} = -\frac{\overline{R}T}{2F} \frac{i_{el,a}}{\left(1 - \frac{p_{H_2}}{p_a}\right) D_{H_2(eff)} + \left(\frac{p_{H_2}}{p_a}\right) D_{H_2O(eff)}} \tag{27b}$$

$$\frac{di_{el,a}}{dx} = -S_{t,a} i_{oo,a} \left\{ \frac{p_{H_2}}{p^I_{H_2}} \exp\left(\beta \frac{n_{e,a} F \eta_{o,a}}{\overline{R}T}\right) - \frac{p_a - p_{H_2}}{p_a - p^I_{H_2}} \times \exp\left[-(1-\beta)\frac{n_{e,a} F \eta_{o,a}}{\overline{R}T}\right] \right\} \tag{27c}$$

The associated boundary conditions are as follows:
for $x = 0$

$$\frac{d\eta_{o,a}}{dx} = -\rho_{el(eff),a} i \quad i_{el,a} = i \quad p_{H_2} = p^I_{H_2}$$

$x = l_a$

$$\frac{d\eta_{o,a}}{dx} = \rho_{io(eff),a} i$$

The overall anode polarization (η_a) can be obtained by integrating these equations simultaneously. These equations do not yield analytical solution; they can only be solved numerically.

Similarly, total polarization of the cathode can be expressed by the following set of differential equations:

$$\frac{d^2\eta_{o,c}}{dx^2} = (\rho_{el(eff),c} + \rho_{io(eff),c}) S_{t,c} i_{oo,c} \times \left\{ \frac{p_{O_2}}{p^I_{O_2}} \exp\left(\beta \frac{n_{e,c} F \eta_{o,c}}{\overline{R}T}\right) - \exp\left[-(1-\beta)\frac{n_{e,c} F \eta_{o,c}}{\overline{R}T}\right] \right\} \tag{28a}$$

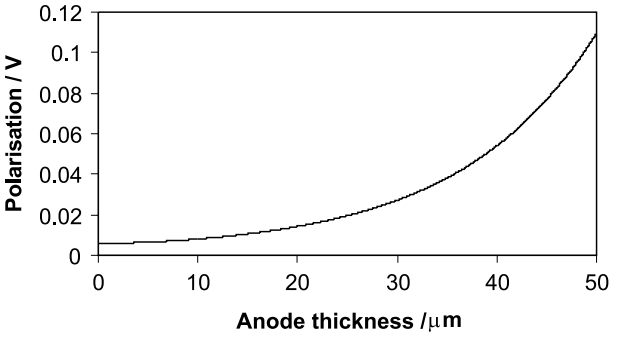

Fig. 8. Polarization distribution along anode when anode is thin (Right side is anode–electrolyte interface).

$$\frac{dp_{O_2}}{dx} = \frac{\overline{R}T i_{el,c}}{4F D_{O_2(eff)} p_c} (p_c - \delta_{o_2} p_{O_2}) \tag{28b}$$

$$\frac{di_{el,c}}{dx} = -S_{t,c} i_{oo,c} \left\{ \frac{p_{O_2}}{p^I_{O_2}} \exp\left(\beta \frac{n_{e,c} F \eta_{o,c}}{\overline{R}T}\right) - \exp\left[-(1-\beta)\frac{n_{e,c} F \eta_{o,c}}{\overline{R}T}\right] \right\} \tag{28c}$$

The associated boundary conditions are
$x = 0$

$$\frac{d\eta_{o,c}}{dx} = -\rho_{el(eff),c} i \quad i_{el,c} = i \quad p_{O_2} = p^I_{O_2}$$

$x = l_c$

$$\frac{d\eta_{o,c}}{dx} = \rho_{io(eff),c} i$$

These equations contain some parameters such as the effective resistivity and the active area per unit volume, which can be obtained using the method proposed by Costamagna et al. [5] who consider the electrodes to be formed by a random packing of spherical powder.

Figure 8 shows the distribution of polarization along a 50 μm thick anode, which operates at 1 A cm^{-2}. It can be seen that the reactions occur throughout the entire anode, although more reaction takes place near anode–electrolyte interface. In this case, the concentration polarization is small due to the use of a thin anode. Since activation polarization is the major loss in the anode, the overall anode polarization, $\eta_{o,a}$, is simply the summation of activation polarization at each reaction layer. Because the individual $\eta_{o,a}$ obeys the Butler–Volmer equation, integration of $\eta_{o,a}$ must also obey the Butler-Volmer equation. Therefore, Equation 5 is applicable when the cermet electrode is thin.

Figure 9 shows the polarization distribution along the anode at 1 A cm^{-2} with anode thickness of 750 μm. It can be seen that almost all reactions take place near the anode–electrolyte interface. In this case, although the anode is thick, the difference in concentration polariza-

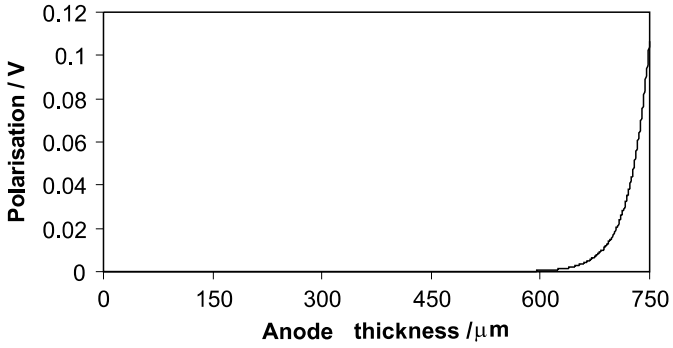

Fig. 9. Polarization distribution along anode when anode is thick (right side is anode–electrolyte interface).

tion at different reaction layers is small. Therefore, under normal fuel cell operating conditions, Equation 5 can also be used for a thick cermet electrode. However, when the current density approaches its limiting value, the situation is quite different. If H_2 cannot diffuse deeply into the electrode, more reaction will take place at outer layer of the anode. Therefore, the predicted polarization would not increase abruptly when approaching the limiting current density. This is why Kim et al. [9] were unable to fit their equation well to the experimental data as shown in Figure 5 of [9], in which the measured voltage did not seem to drop steeply as compared with the curve-fitted data when approaching the limiting current density.

Arising from the above analysis, it can be concluded that system Equations 18 can be used in a general analysis of SOFC, in particular for electrode performance and fuel cell system study.

6. Concentration resistance analysis

Current density dependent area-specific resistance of the cell is the negative gradient of the $E(i)$ against i curve, where the contribution of concentration polarization to the cell resistance is

$$R_{\mathrm{Conc}}(i) = \frac{\overline{R}T}{4F}\frac{\frac{\overline{R}T}{4F}\frac{l_c}{D_{c(\mathrm{eff})}}\frac{(p_c/\delta_{O_2}-p^{\mathrm{I}}_{O_2})}{p_c/\delta_{O_2}}\exp\frac{\overline{R}T}{4F}\frac{\delta_{O_2}l_c}{D_{c(\mathrm{eff})}p_c}i}{\frac{p_c}{\delta_{O_2}}-\frac{p_c}{\delta_{O_2}}-p^{\mathrm{I}}_{O_2}\exp\frac{\overline{R}T}{4F}\frac{\delta_{O_2}l_c}{D_{c(\mathrm{eff})}p_c}i} + \frac{\overline{R}T}{2F}\frac{\frac{\overline{R}T}{2F}\frac{l_a}{D_{a(\mathrm{eff})}}}{p^{\mathrm{I}}_{H_2}-\frac{\overline{R}T}{2F}\frac{l_a}{D_{a(\mathrm{eff})}}i} + \frac{\overline{R}T}{2F}\frac{\frac{\overline{R}T}{2F}\frac{l_a}{D_{a(\mathrm{eff})}}}{p^{\mathrm{I}}_{H_2O}+\frac{\overline{R}T}{2F}\frac{l_a}{D_{a(\mathrm{eff})}}i} \tag{29}$$

In this equation, the last two terms on the right hand side are related to the inlet partial pressure of H_2 and H_2O. A function $F(p^{\mathrm{I}}_{H_2})$ is defined as follows:

$$F(p^{\mathrm{I}}_{H_2}) = \frac{1}{p^{\mathrm{I}}_{H_2}-\frac{\overline{R}T}{2F}\frac{l_a}{D_{a(\mathrm{eff})}}i} + \frac{1}{(p_a-p^{\mathrm{I}}_{H_2})+\frac{\overline{R}T}{2F}\frac{l_a}{D_{a(\mathrm{eff})}}i} \tag{30}$$

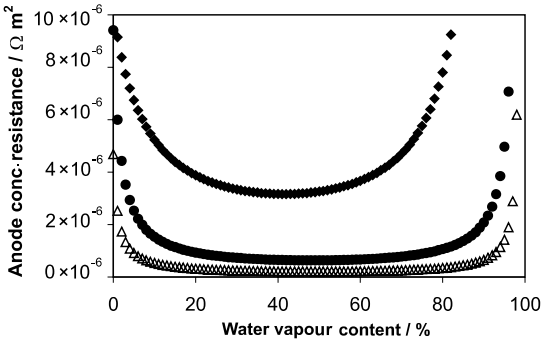

Fig. 10. Effect of water vapour content on anode concentration resistance. (Assuming $p_a = 1$ atm, $T = 1073$ K, $i = 0.5$ A cm^{-2}, $D_{a(\mathrm{eff})} = 0.2 \times 10^{-4}$ m^2 s^{-1} and anode thickness is 750 (◆), 150 (●), 50 (△) μm, respectively).

where $p^{\mathrm{I}}_{H_2O} = p_a - p^{\mathrm{I}}_{H_2}$.

The second derivative of $F(p^{\mathrm{I}}_{H_2})$ with respect to $p^{\mathrm{I}}_{H_2}$ shows that the function contains a minimum point. Thus, when $(\mathrm{d}F(p^{\mathrm{I}}_{H_2})/\mathrm{d}p^{\mathrm{I}}_{H_2}) = 0$, we obtain

$$p^{\mathrm{I}}_{H_2} = \frac{p_a}{2} + \frac{\overline{R}T}{2F}\frac{l_a}{D_{a(\mathrm{eff})}}i \tag{31a}$$

$$p^{\mathrm{I}}_{H_2O} = \frac{p_a}{2} - \frac{\overline{R}T}{2F}\frac{l_a}{D_{a(\mathrm{eff})}}i \tag{31b}$$

Therefore, if the fuel is humidified according to Equation 31(b), the resistance of the cell due to the anode concentration polarization will be minimal.

Figure 10 shows the effect of water vapour content on the anode concentration resistance. High anode concentration resistance is obtained when pure H_2 is used. The resistance drops significantly when a small amount of water vapour is added to the H_2. The resistance does not seem to change greatly over a wide range of H_2 partial pressures. For example, when the anode thickness is 50 μm, adding about 10% of water vapour could yield negligible anode concentration resistance. The minimum resistance, in the case of a thick anode, occurs when the water vapour content is about 40%. It can also be seen that the thicker the anode, the higher the resistance.

References

1. E.A. Liese and R.S. Gemmen, ASME Paper 99-GT-360 (1999).
2. S.E. Veyo and W.L. Lundberg, ASME Paper 99-GT-356 (1999).
3. D.J. White, ASME Paper 99-GT-419 (1999).
4. P.F. van den Oosterkamp, A.A. Goorse and L.J.M.J. Blomen, *J. Power Sources* **41** (1993) 239–252.
5. P. Costamagna, P. Costa and V. Antonucci, *Electrochim. Acta* **43** (1998) 375.
6. S.H. Chan and Z.T. Xia, *J. Electrochem. Soc.* **148** (2001) A388–A394.
7. S.H. Chan, K.A. Khor and Z.T. Xia, *J. Power Sources* **93** (2001) 130.
8. J.H. Hirschenhofer, D.B. Stauffer, R.R. Engleman and M.G. Klett, 'Fuel Cell Handbook', 4th edn., Department of Energy, USA (1998).
9. J.W. Kim, A.V. Virkar, K.Z. Fung, K. Mehta and S.C. Singhal, *J. Electrochem. Soc.* **146** (1999) 69.
10. K. Huang, B. Tichy and J.B. Goodenough, *J. Am. Ceram. Soc.* **81** (1998) 2581.
11. R. Maric, S. Ohara, T. Fukui, H. Yoshida, M. Nishimura, T. Inagaki and K. Miura, *J. Electrochem. Soc.* **146** (1999) 2006.
12. T. Ishihara, M. Honda, T. Shibayama, H. Minami, H. Nishiguchi and Y. Takita, *J. Electrochem. Soc.* **145** (1998) 3177.